Cryogenics 108 (2020) 103070

Contents lists available at ScienceDirect

Cryogenics

journal homepage: www.elsevier.com/locate/cryogenics

Research paper

Electromagnetic behaviour and thermal stability of a conduction-cooled, no-insulated 2G-HTS coil at intermediate temperatures

A. Cubero, A.B. Núñez-Chico, R. Navarro, L.A. Angurel, E. Martínez*

Instituto de Ciencia de Materiales de Aragón (CSIC – Universidad de Zaragoza), C/ María de Luna 3, 50018 Zaragoza, Spain

ARTICLE INFO

Keywords:
Superconductor
HTS no-insulation coils
Conduction-cooling
Thermal stability
Thermal contact conductance
Coil losses

ABSTRACT

The electromagnetic and thermal properties of a double pancake coil made of second generation high temperature superconductor, 2G-HTS, have been studied. The coil was wound with no-insulation between turns (NI coil) and was later impregnated with epoxy resin and glued to a copper support plate. The coil was thermally anchored to the cryocooler cold finger and cooled by conduction. After several thermal cycles no degradation of its superconducting properties was observed.

The coil was operated under high vacuum and high currents (up to 400 A in steady conditions) at different temperatures in the range between 5 K and 77 K, with special focus on the analysis above 30 K. The charge and discharge characteristics, and the experimentally measured and numerically estimated critical currents, have been studied. The different loss contributions during current ramp and the thermal contact conductance between different parts of the double pancake coil have been measured. The implications of these two factors on the thermal stability and the behaviour of the whole cryogenic system are discussed.

1. Introduction

Superconducting coils based on high temperature superconductors (HTS) are of great interest for their possible use in electric power applications, such as superconducting generators, motors, magnetic energy storage systems, etc. [1–4]. Also they may offer important advantages compared to low-temperature superconducting (LTS) coils. Some examples of traditional and well-established LTS applications are resonance magnetic imaging, nuclear magnetic resonance and high-energy particle accelerators. HTS would allow higher operating temperatures or magnetic fields, eliminating the requirement of liquid helium in certain commercial applications [5–7].

Superconducting magnets may suffer from quench during operation, that is, the irreversible superconducting-to-normal transition of the coil, which could cause a permanent damage if it is not appropriately handled. No-insulated (NI) coils, without turn-to-turn insulation, have been the subject of intense research in the last few years [8–15], especially those based on second generation high temperature superconductors, 2G-HTS. NI coils reach greater compactness than the standard ones, and are more robust against thermal instabilities [16]. Thus, they would enable safer operation at large currents, preventing possible coil degradation in case of quench. On the contrary, they present a delay between the field and the current ramp that can be a drawback for certain applications.

Since HTS and MgB_2 coils are usually designed to operate at temperatures above 20 K, they can be cooled by direct thermal contact with the cryocooler cold head [10,13,14,17–20]. Thus, no liquid helium would be needed, unlike traditional low temperature superconducting magnets, although cryogen-free LTS working at 4–10 K [21,22] as well as hybrid magnets [23–24] have also been built and tested. Achieving high thermal conductance values between the cryocooler and the whole system, including current leads and current contacts, is crucial. Otherwise, thermal runaway can occur if the system is not sufficiently thermalized. Since this is more critical for high operating currents, the range of 100–200 A has been usually chosen for conduction-cooled HTS magnets [10,13,14,17–19]. Nevertheless, due to the high price of the HTS conductors, increasing the operating current even at the expense of certain reduction in the operating temperature, would reduce the cost, as less length of conductor would be necessary.

The aim of the present work is to analyse the superconducting behaviour of a 2G-HTS NI double pancake coil and its thermal stability under conduction-cooling conditions. The coil has been energized with high currents, up to around 450 A, and operated at variable temperatures, focusing on intermediate temperatures between 30 K and 60 K. The critical current values have been estimated numerically and compared with the experimental values. The characteristic parameters of the coil as a function of the temperature, such time constants during

* Corresponding author.
E-mail address: elenamar@unizar.es (E. Martínez).

https://doi.org/10.1016/j.cryogenics.2020.103070
Received 28 October 2019; Received in revised form 6 March 2020; Accepted 16 March 2020
Available online 23 March 2020

Table 1
Characteristics of the 2G-HTS tapes and double-pancake coil.

Conductor used	2G-HTS, SuperPower Inc SCS4050-AP Ref. M4-180-4 0508
Width (w)/Thickness/Total length	4 mm/163 μm/14 m
Coil geometry	Round, double pancake
Impregnation	Stycast 1266 (after dry winding)
Insulation between turns	Bare
Diameter inner/outer (D_{in}/D_{out})	67 mm/77 mm
Distance between pancake coils	1 mm
Number of turns	30 × 2
Magnetic field per ampere at centre	0.985 mT/A (Experimental) 1.035 mT/A (Simulation)
Max. field per ampere in the winding	3.5 mT/A (Simulation)
Inductance, L	0.386 mH (Experimental) 0.406 mH (Simulation)

charge and discharge tests, as well as the characteristic resistance of the coil, have been analysed. The effect of thermal cycling in the superconducting and thermal properties of the coil has also been analysed.

2. Experimental

2.1. Characteristics of the double pancake 2G-HTS coil

A double pancake (DP) coil, without electrical contact resistance between both pancake coils, was manufactured using 2G-HTS conductors provided by SuperPower Inc. The main characteristics of the used tape and fabricated coil are collected in Table 1. The conductor has a critical current I_c = 124 A at 77 K and self-field. It has a width of 4 mm and a total thickness of 163 μm (including the 50-μm Hastelloy substrate and 110-μm total thickness of copper stabilizer). Each pancake coil has 30 turns and the distance between the upper and lower coil is 1 mm. The coil was dry-wound around a 304L stainless steel cylinder of 67 mm diameter and 0.3 mm thickness, which acts as mechanical support. No-insulation between turns was used. During winding, several thin copper sheets were soldered to the HTS conductor to easily solder voltage taps and thermocouples after coil fabrication. Subsequently, it was impregnated with Stycast-1266 epoxy resin, which has low viscosity. Stycast-2850 FT, which has higher thermal conductivity and viscosity, was used to glue the DP coil to a 2-mm thick copper plate and to fill the gap between both pancake coils. The copper support plate was mechanically anchored to the second stage of the cryocooler ensuring a good thermal contact between them.

The coil was instrumented using several voltage taps and two thermocouples, as shown schematically in Fig. 1. The measured voltages are named as follow. V_{COIL} is the total voltage of the DP coil; V_{Low} and V_{Up} the voltages of the lower and upper pancake coils, respectively. The voltage of the innermost turn (#1) of the upper pancake coil, $V_{U\text{-}1}$, was also measured to rule-out any possible damage during fabrication.

A Hall probe is installed at the centre of the DP coil to measure the axial magnetic field, B_{centre}. Two thermocouples, TC-up and TC-low, were placed in the outermost turns of the upper and lower pancake coils, respectively. Moreover, to measure the thermal contact conductance between both pancakes and between the lower coil and the copper support plate, a manganin heating wire with resistance of 5 Ω was glued to the top surface of the coil using GE varnish, as shown in Fig. 1(b).

2.2. Experimental set-up

An experimental set-up was developed to test superconducting devices cooled by conduction at variable operating temperatures and currents up to 500 A. The analysed devices are in high vacuum and thermally anchored to the second stage of a cryocooler (SRDK-415D, Sumitomo). The system enables variable operating temperatures, T, from 5 K to 77 K, controlled by means of an additional heater and a Lakeshore temperature controller.

The voltages between different taps of the coil and current leads, the Hall probe and thermocouple signals were recorded using a data acquisition device, which is controlled by a LabView program. Two Agilent DC power supplies were used for these experiments, one provides maximum currents and voltages of 100 A and 20 V, and the other of 875 A and 5 V.

2.3. Current leads

Current leads, which connect room temperature (RT) to the coil, were designed to work in vacuum at operating currents up to 400 A (in steady conditions) and at 500 A (for pulses of several seconds). In order to minimize the heat input into the superconducting device, each current lead has three sections whose ends are connected by bolted joints that are thermally anchored to three heat sinks per lead, HS0, HS1 and HS2, as it is shown in Fig. 2(a). Electrical insulation is achieved by coating the Cu with an alumina layer. HS0 is thermally anchored to the 2nd stage of the cryocooler (cold finger) and HS1 to the 1st stage. The coldest section of the current lead (between HS1 and HS0 sinks) is a commercial HTS current lead from HTS-110, made from 1st generation HTS wires with an alloyed matrix used to minimise the thermal conductivity. The other sections were fabricated with copper. A small liquid nitrogen (LN) vessel was built inside the cryostat to add some extra

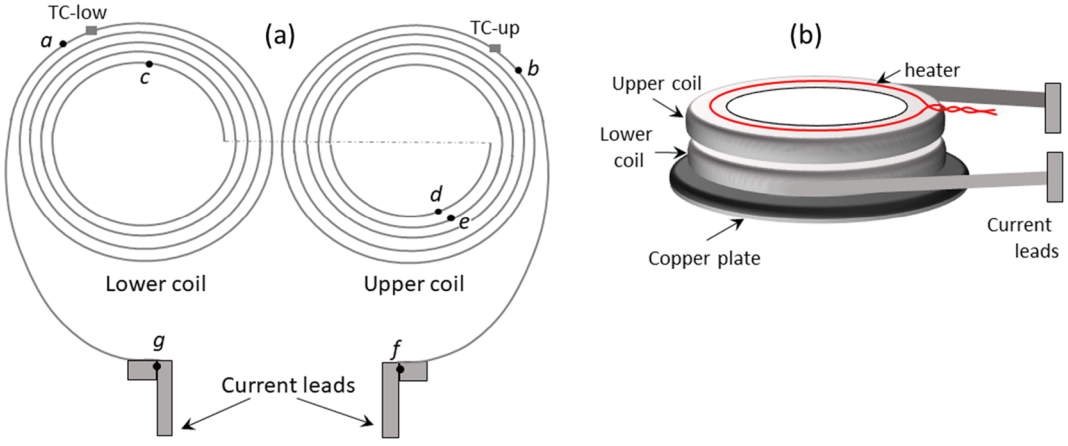

Fig. 1. (a) Scheme of the voltage tap positions and thermocouples within the double pancake coil (only few turns are drawn for clarity purposes). Both points connected by the discontinuous line in this drawing correspond to the same point in the real DP coil. The voltage of the total coil, V_{COIL}, was measured with taps a and b; voltages of the upper (V_{Up}) and lower (V_{Low}) pancake coils with taps d-b and a-c, respectively. $V_{U\text{-}1}$ (d-e) is the voltage of turn #1 (the innermost turn) of the upper coil. (b) Schematic 3D view of the DP coil with the heater glued at the top surface of the coil.

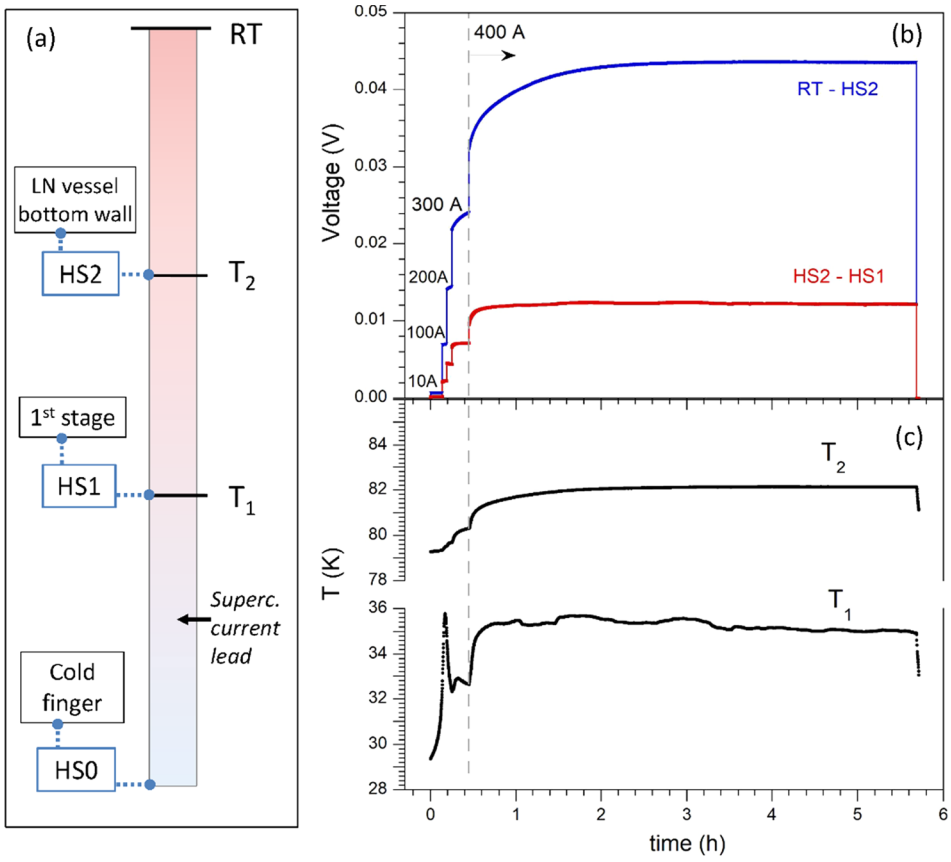

Fig. 2. (a) Scheme of the thermal links of each current lead with the heat sinks HS2, HS1 and HS0. (b) Time evolution of the voltages measured in the current lead copper sections between room temperature (RT) and HS2, and between HS2 and HS1 for DC applied currents up to 400 A. (c) Temperatures $T_2(t)$ and $T_1(t)$ measured at the positions of the current lead in thermal contact to HS2 and HS1 sinks, respectively.

refrigeration power, since the cooling power of the used cryocooler is not sufficient to achieve temperatures below 70–77 K in the 1st stage, for currents of 500 A. Note that the theoretical minimum heat input value of a metal current lead between 300 K and 77 K in vacuum conditions is ≈ 0.04 W/A (per lead) [25]. The sink HS2 is in thermal contact with the LN vessel, bolted to the outer surface of the bottom of the vessel, i.e. it is neither immersed in the liquid nor cooled by interchange gas.

Considering Ekin predictions [25] and using finite element software COMSOL, the current leads were optimised for steady operating currents of 400 A. The warmer section of each current lead consists of a copper cylinder (25 cm length, 1 cm diameter) soldered to a copper braided wire (13 cm length, 25 mm^2 cross sectional area), which ends in HS2. The part between HS2 and HS1 is a Cu braided wire of 30 cm length and 25 mm^2 section. At 400 A, the estimated heat inleak values into the heat sinks HS2 and HS1 are 14.7 W and 5 W, respectively, per lead. Moreover, the numerically calculated heat loads in each lead due to ohmic losses are 15 W (in the lead section between RT and HS2), and 3.5 W (between HS2 and HS1 heat sinks).

Different experiments were performed to test the current leads before measuring the superconducting coil. Fig. 2 shows the time evolution of voltages in the current lead copper sections and temperatures $T_1(t)$, and $T_2(t)$, measured in the lead at the thermal joints to HS1 and HS2, respectively, for different values of the applied current ranging from 10 A to 400 A. It is observed that the system achieves steady conditions, although the equilibrium in the section between HS2 and HS1 is reached considerably faster than in the warmer section (between RT and HS2). The larger temperature differences between this lead section ends, together with the greater copper mass and the higher heat capacity of the warmer section, explain this behaviour. Therefore, this would be the most critical part of the current lead. The smooth evolution of $T_2(t)$ for all applied currents contrasts with the oscillations of $T_1(t)$, which might be due to refrigeration fluctuations of the cryocooler compressor. These fluctuations were not observed in the second stage and do not affect the thermal stability of system. The current is kept constant by the power supply.

At equilibrium conditions, the measured heat loads due to ohmic losses at 400 A were 17.5 W per lead (in the section between RT and HS2) and 4.8 W (between HS1 and HS2). These values are of the order but systematically higher than the numerical predictions, probably due to underestimations of the electrical contact resistances between the different sections of the lead. The values of the thermal contact conductance of the electrically insulated joints at the heat sinks, h_j, have been estimated as:

$$h_j = \frac{1}{A_c}\frac{\dot{Q}}{\Delta T}, \tag{1}$$

where $\dot{Q}$ is the numerically calculated total heat inleak into the heat sink, ΔT is the measured temperature difference across the thermal joint in steady state conditions, and A_c is the contact area of the joint. We have obtained values of $h_j \approx 850$ and 1800 W m^{-2} K^{-1} for HS1 ($A_c = 20$ cm^2) and HS2 ($A_c = 17$ cm^2), respectively.

3. Results and discussion

3.1. Charge and discharge tests

Charge and discharge tests of the coil have been performed at operating temperatures from 5 K to 77 K and currents well below I_c. A typical test at two different current ramp rates (10.3 A/s and 3.4 A/s) is displayed in Fig. 3. Once reached the set current of 98 A, it was kept constant during several seconds and, subsequently, switched-off (sudden discharge).

The electrical behaviour of the NI coil has been modelled [9] by a simple equivalent circuit consisting of two impedances in parallel, and thus the applied current, $I(t)$, divides in two paths: One carries the

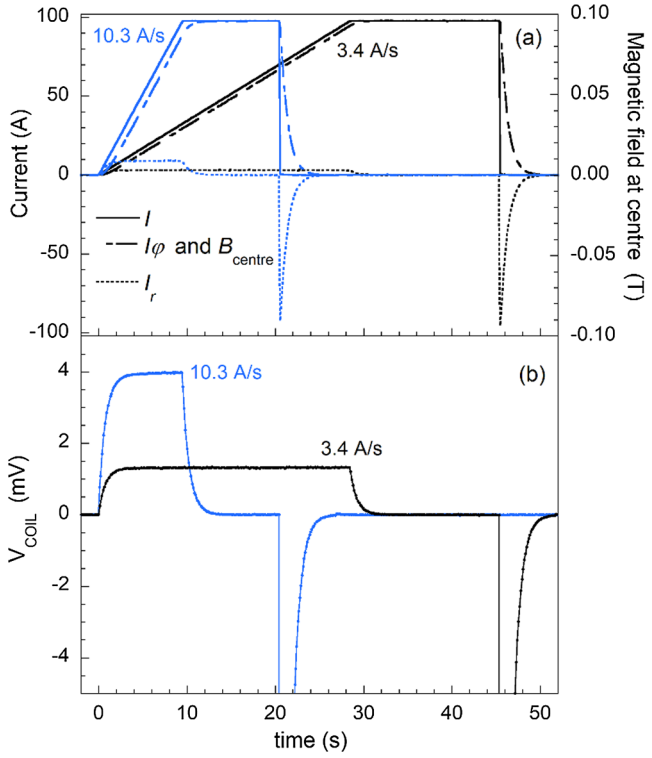

Fig. 3. Charge and discharge tests of the NI coil at 30 K, up to 98 A, for two different charging rates (10.3 and 3.4 A/s): (a) Applied current, $I(t)$, axial magnetic field at the coil centre, $B_{centre}(t)$, and estimated $I_\varphi(t)$ and $I_r(t)$ curves. (b) Coil voltage $V_{COIL}(t)$ measured during the experiment. Note that the scale has been cut-off for better observation of the voltage during charge.

current along the spiral conductor path, I_φ (t), and its impedance is given by the coil self-inductance, L, in series with a current-variable resistance, $R_\varphi(I_\varphi)$. The other is the equivalent resistance, R_r, which would be mainly determined by the turn-to-turn electrical contacts and carries the current in the radial direction of the coil, $I_r(t)$. The Kirchhoff and charge conservation laws relate the parameters of the equivalent circuit to $I(t)$ and the coil voltage, $V_{COIL}(t)$, by Eqs. (2)–(3). Due to the axial symmetry of the coil, $I_r(t)$ does not contribute to the magnetic field, and, in consequence, the magnetic field is proportional to I_φ, Eq. (4). The constant k is fixed by the geometry of the coil and does not change with temperature.

$$V_{COIL}(t) = R_r I_r(t) = L\frac{dI_\varphi(t)}{dt} + R_\varphi(I_\varphi)I_\varphi(t) \tag{2}$$

$$I(t) = I_r(t) + I_\varphi(t) \tag{3}$$

$$I_\varphi(t) = \frac{B_{centre}(t)}{k} \tag{4}$$

The current dependence of $R_\varphi(I_\varphi)$ is caused by current sharing between the thin superconductor layer and the metallic components of the 2G-HTS tape conductor. It takes into account the non-linear I-V behaviour of the superconductor and the ohmic resistance of the metallic components [8,9].

According with these equations, k was firstly determined experimentally from the magnetic field at the coil centre, B_{centre}, measured at constant current and steady conditions ($I_\varphi = I$), obtaining $k = 0.985(5)$ mT/A for the analysed DP coil. $I_\varphi(t)$ was derived from Eq. (4); and $I_r(t)$ using Eq. (3). Finally, from $I_\varphi(t)$ and $I_r(t)$, the values of L and R_r can be estimated from the experimental $V_{COIL}(t)$ values using Eq. (2).

The $B_{centre}(t)$, $I(t)$ and $V_{COIL}(t)$ curves directly measured, and $I_\varphi(t)$ and $I_r(t)$ currents derived from the above equivalent circuit equations, are displayed in Fig. 3. The higher the current ramp rates, the larger the maximum values of $I_r(t)$, in consonance with longer time delays between $I(t)$ and $B_{centre}(t)$. For these conditions, the maximum I_r values were 9 A and 3 A for 10.3 A/s and 3.4 A/s, respectively. Moreover, values of $L = 0.386$ mH and $R_r = 0.44$ mΩ were estimated at 30 K. During the linear ramp, after a transient, $V_{COIL}(t)$ becomes constant, with values increasing proportionally with the applied current ramp rate. When the set current is reached, after a similar transient time, $B_{centre}(t)$ becomes constant and $V_{COIL}(t)$ zero, indicating that all the current flows through superconducting paths, with the entire coil below I_c.

The sudden switch-off of the applied current, which has a characteristic time constant of about 10 ms, produces an exponential decay of $B_{centre}(t)$ with much larger time constants, $\tau \approx 860$ ms at 30 K. It also produces sharp negative peaks of the coil voltage ($V_{COIL} \approx -60$ mV in this case) and turn-to-turn flowing current inverse to I_φ ($I_r = -I_\varphi = -98$ A), followed by an exponential relaxation (Fig. 3). In these conditions, the sudden coil discharge produced a temperature rise of $\approx$ 0.5 K (measured by the thermocouple TC-up).

For further analysis of the adequacy of the used equivalent circuit, it is interesting to evaluate the electric energy loss, $Q_{loss}(t)$, given by:

$$Q_{loss}(t) = Q_{in}(t) - Q_m(t) \tag{5}$$

where $Q_{in}(t)$ is the energy supplied to the coil from the beginning of the current ramp ($t = 0$) to the time t; and $Q_m(t)$ is the magnetic energy stored in the coil at time t:

$$Q_{in}(t) = \int_0^t V_{COIL}(t)I(t)dt \tag{6}$$

$$Q_m(t) = \frac{1}{2}LI_\varphi^2(t) \tag{7}$$

Moreover, the energy dissipated by the currents flowing in the radial direction during the ramp is estimated by:

$$Q_r(t) = \int_0^t \dot{Q}_r(t)dt = \int_0^t R_r I_r^2(t)dt \tag{8}$$

Fig. 4 shows $Q_{loss}(t)$, $Q_{in}(t)$, $Q_m(t)$ and $Q_r(t)$, calculated using Eqs. (5)–(8) from the measurements at 30 K, ramp rate of 10.3 A/s up to 98 A, already displayed in Fig. 3. It is worth mentioning the good correspondence between $Q_{loss}(t)$ and $Q_r(t)$. This behaviour, which was also observed for ramp rate of 3.4 A/s, indicates that the main energy loss contribution during charging is due to the turn-to-turn current, whereas the magnetization loss [26] is negligible for these conditions. The electric energy loss during the whole ramp up to 98 A decreases from 0.3 J (for 10.3 A/s) to 0.11 J (for 3.4 A/s). The power losses due to turn-

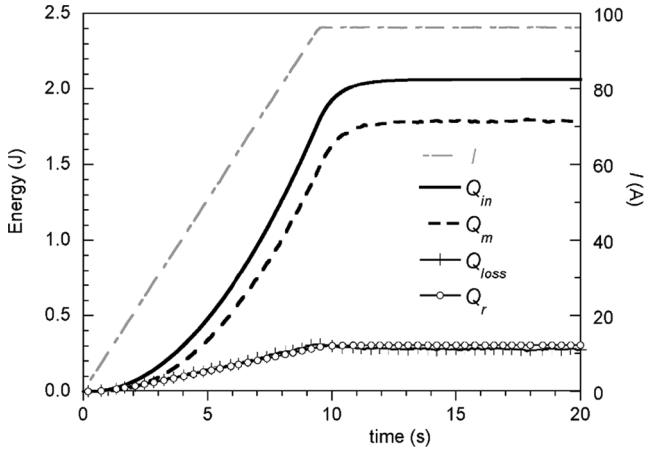

Fig. 4. Total energy supplied to the coil at 30 K, $Q_{in}(t)$, energy loss, $Q_{loss}(t)$, magnetic energy stored in the coil, $Q_m(t)$, and energy dissipated by the currents flowing in the radial direction, $Q_r(t)$, when the current is linearly ramped up to 98 A at 10.3 A/s, calculated using Eqs. (5)–(8) from the experimental results in Fig. 3.

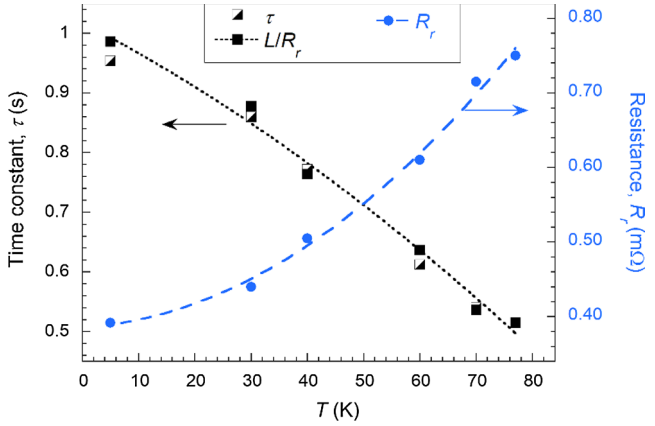

Fig. 5. Temperature dependence of the exponential decay time constant, τ, of the magnetic field, B, in case of sudden discharges of the coil; equivalent radial resistance, R_r, estimated experimentally during coil charging; and corresponding L/R_r values for $I < I_c$. Dashed and dotted lines are 2nd order polynomial fits to guide the eye.

to-turn current, $\dot{Q}_r$, reach maximum values of 36 mW (for 10.3 A/s) and 4 mW (for 3.4 A/s) during the same ramp. The balance between the electric power loss and the conduction cooling power results in a small temperature increment of 0.1 K (measured by TC-up) at the end of the current ramp up to 98 A for the rate of 10.3 A/s, but no temperature increase was measured for 3.4 A/s. This is the reason why the latter was chosen to estimate experimentally the critical current of the coil, as it will be seen in Section 3.3.

The time constant $\tau(T)$ obtained from the magnetic field decay for sudden discharges of the coil at different temperatures is plotted in Fig. 5, together with the equivalent resistance $R_r(T)$ and the $L/R_r(T)$ ratio estimated from Eqs. (2)–(4). Since the experimentally obtained L values are almost constant between 5 K and 77 K (L = 0.386 mH, ± 2%), the temperature variation of the characteristic time constant $\tau(T)$ is only due to $R_r(T)$. Note that $R_r(T)$ almost doubles from 5 K to 77 K, in good agreement with the reported temperature dependence of electric contact resistance between two single 2G-HTS tapes [27].

From the deduced equivalent resistance in the radial direction R_r, it is possible to estimate the turn-to-turn electrical contact resistance, R_t, assuming that this is homogeneous for all turns, so that:

$$R_r = 2\sum_{i=1}^{N} \frac{R_t}{2\pi r_i w} \quad (9)$$

where N is the number of turns of each pancake, r_i is the radius of i-turn and w is the tape width. At 77 K, the obtained R_r = 0.74 ± 0.01 mΩ, would then correspond to $R_t \approx 110$ μΩ cm^2.

The values of R_t for NI coils would depend on many factors, such as the tape surface condition (oxidation and roughness), the use of metal cladding between turns, the resin impregnation or the winding tension [9,11,13,26,27]. At 77 K, reported R_t values typically range between 10 and 100 μΩ cm^2. The estimated value obtained in this work is thus in this range, but in the upper bound, probably due to the use of Stycast after winding, although this does not alter significantly the behaviour observed for non-impregnated coils.

3.2. Numerical estimation of the coil critical currents at different temperatures

For design purposes, as well as to prevent damaging the coil during testing, it is very useful to have an estimation of the expected critical currents of the coil at different temperatures. The load-line method has been commonly used in LTS coils to calculate their critical current [28]. This method compares the calculated maximum magnetic field in the winding at different operating currents, with the I_c-B isotherms measured in a single conductor. By plotting these values together, the crossing points would give the coil's critical current value at each temperature. In case of HTS, this procedure is not as straightforward as in LTS. This is because critical current of HTS does not only depend on the magnitude of the magnetic field, B, but also on the orientation of this field with respect to the tape surface, θ. Moreover, $I_c(\theta)$ depends on temperature and field [29].

Different methods have been proposed to estimate the critical current of HTS coils [29–31]. In this work, we used a method similar to the so-called "modified load-line method" in [31], which takes into account the anisotropy of the superconductor. As for the conventional load-line method, the first step is to calculate the magnetic field inside the winding for a given applied current, I, assuming that the current distributes uniformly in the winding. Fig. 6(a) shows the magnetic flux lines and the field amplitude inside the winding calculated for I = 475 A. As it is observed in the figure, for a particular turn (fixed x value), the amplitude and orientation of the magnetic field vary significantly along the z direction, i.e. along the width of the tape. The field gradient across the tape thickness, d, was not considered here because, due to the geometry of these conductors ($d \ll w$), it would be much less relevant. For each turn, $B(z)$ and $\theta(z)$ curves can be obtained from Fig. 6(a) for a given operating current. With these data and by using the dependence on (B,θ,T) of the critical current per unit width, I_c/w, previously

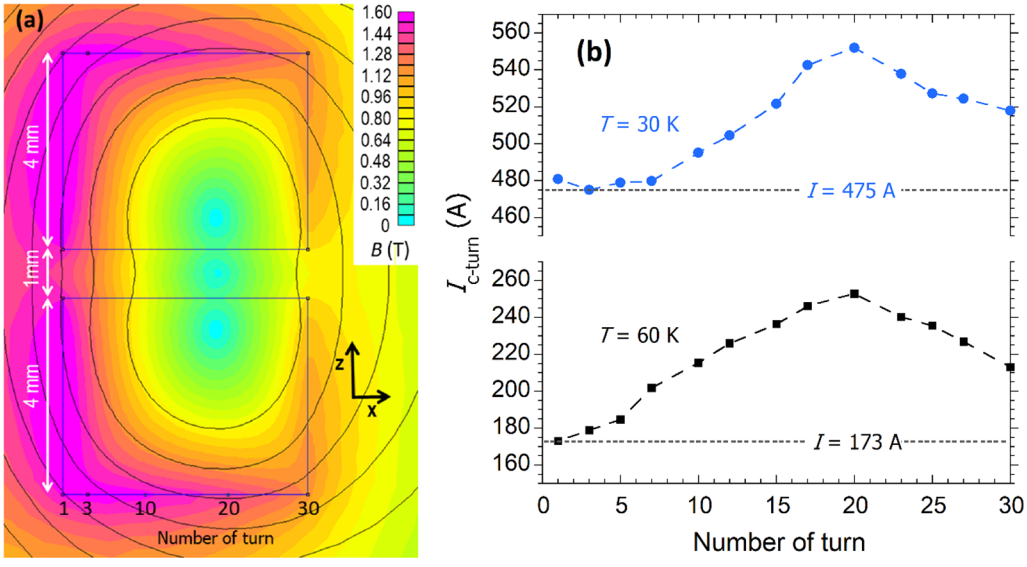

Fig. 6. (a) Magnetic field distribution and flux line plot of the DP coil for I = 475 A, calculated using FEMM software considering uniform current densities. Turns "1" and "30" correspond to the innermost and the outermost turns, respectively. b) Critical currents of several turns, $I_{c\text{-turn}}$, calculated at 30 K and 60 K for applied currents of 475 A and 173 A, respectively.

measured in a similar short sample (SuperPower Inc, SCS4050-AP, M4-134-3) [32], the local $(I_c/w)(z)$ values can be calculated for each turn. The integration of these values along the width of the tape would give an estimation of the critical current of each turn, $I_{c\text{-turn}}$. Note that this assumption is an approximation to the critical state model behaviour. This process is repeated for different current values. Analogously to the standard load-line method, the minimum of all $I_{c\text{-turn}}$ values, coincident with the applied current, would give the critical current of the coil.

Fig. 6(b) shows the calculated critical currents of several turns at temperatures of 30 K and 60 K and applied currents $I = I_c = 475$ A and 173 A, respectively. It must be remarked that in both cases the innermost turns limit the critical current of the coil. This is because this region has the lower local critical currents, whereas the coil zone around turn number 20 has the highest critical current, which coincides with the lowest magnetic field region. Similar behaviour has been observed experimentally in single pancake coils fabricated with similar coated conductors [33]. As it can be seen in the figure, the distribution of local critical currents inside the winding depends on the temperature, because so does $I_c(B,\theta)$. It is worth mentioning that although for self-field conditions, as considered here, the innermost turns become typically critical before the rest of the coil, this is not always the case for 2G-HTS coils due to the relevance of the specific $I_c(B,\theta)$ behaviour of the used tape [31]. The validity of the assumptions used in the modeling will be discussed further below.

3.3. Experimental critical currents of the DP coil at different temperatures

To estimate experimentally the critical current of the coil, the current was ramped up at rates of 3.0 or 3.3 A/s up to a set value, held constant for several seconds and subsequently set to zero. The voltages in different regions of the coil were measured during these experiments, which were performed at different temperatures from 70 K down to 30 K. At each temperature, several current ramps were applied. The maximum current of the ramp was increased progressively in different runs. If the ramp current exceeds the local critical current in any part of the winding, a significant increase in the coil voltage will be measured. In this case, a resistive component of the coil voltage will be seen when the current is held constant after the ramp, unlike the purely inductive behaviour observed in Fig. 3(b) when the applied current is well below I_c.

As an example of this behaviour, Fig. 7 displays the obtained results when ramping the current up to 159 and 447 A, at 60 K and 30 K, respectively. The figure shows the applied current; the magnetic field at coil centre; the voltages $V_{Up}(t)$, $V_{Low}(t)$ and $V_{U\text{-}1}(t)$; and temperature $T_{Up}(t)$, measured by the thermocouple placed in the upper coil.

As it is seen in Fig. 7(b) and (f), when ramping-up the current, the voltages measured in the upper and lower coils have initially an inductive component (with almost constant values of about 0.6 mV). But once reached a certain current value during the ramp, voltage $V_{Up}(t)$ increases significantly, indicating that the applied current has exceeded the local critical current in this part of the coil. These resistive signals can be easily visualised when the current is held constant after the ramp. In the conditions of Fig. 7, resistive signals were observed in fact in both pancakes, but with V_{Up} always considerably higher than V_{Low}, which indicates that the upper coil has lower critical current than the lower one. For example, at 60 K and 159 A, $V_{Up} \approx 280$ μV and $V_{Low} \approx 25$ μV were measured (Fig. 7(b)). Besides, the voltage of the innermost turn of the upper coil, $V_{U\text{-}1}(t)$, also shows a transition to the resistive regime during the ramp, with $V_{U\text{-}1} \approx 31$ μV after the ramp (Fig. 7(c)), which is significantly smaller than V_{Up}. This indicates that several turns are above their local I_c values, especially at low temperatures, which is in agreement with numerical estimations of Fig. 6(b), showing several turns with similar $I_{c\text{-turn}}$ in the inner part of the coil. Note that at 60 K, there was a small irregularity in the current ramp linearity at $t \approx 54.4$ s, which produced an additional inductive contribution in the voltages, without further consequences.

Fig. 7(d) and (h) shows the time evolution of the temperature $T_{Up}(t)$ during the experiments at 60 K and 30 K, respectively. In the first case, the temperature remains constant during most of the current ramp, but begins to increase in the later stages of the ramp and continues rising when the current is kept constant. The appearance of resistive losses when current exceeds the local critical current caused a coil temperature increment $\Delta T_{Up} \approx 0.3$ K during the entire experiment. Note that the increase of $T_{Up}(t)$ finishes at the beginning of coil discharge, with a delay of about 4–6 s, which is also observed in the experiment at 30 K.

At 30 K, there is no appreciable temperature increase in the initial stages of the ramp ($t < 55$ s, $I < 150$ A), but later the temperature starts rising and reaches $\Delta T_{Up} \approx 0.3$ K at $t \approx 135$ s ($I \approx 420$ A). Finally, T_{Up} increases sharply, and so does V_{Up}. In order to further analyse the behaviour of the coil at 30 K, Fig. 8 shows the time dependence of the total energy provided to the coil during the ramp, $Q_{in}(t)$, together with other relevant energy curves, $Q_{loss}(t)$, $Q_m(t)$ and $Q_r(t)$, calculated using Eqs. (5)–(8). In this case, it is clearly seen that $Q_{loss}(t)$ is higher than the turn-to-turn loss contribution, $Q_r(t)$. For example, at the end of the current ramp $Q_{loss} = 2.75$ J while $Q_r = 0.46$ J. As it is shown in the inset of Fig. 8, this is because the loss power produced in the superconducting tapes, $\dot{Q}_{sc}$, becomes relevant for these conditions, where:

$$\dot{Q}_{sc}(t) = \left(V_{COIL}(t) - L\frac{dI_\varphi(t)}{dt}\right)I_\varphi(t) = R_\varphi(I_\varphi)I_\varphi^2(t) \tag{10}$$

For the slow current ramp used here, this loss power component becomes increasingly relevant upon increasing the current. For $I < I_c$, this term gives the losses produced in the superconductor, which is subjected to variable current and variable magnetic field during the ramp. When the current is close or exceeds the critical current, the resistive contribution of the metallic elements of the tapes is added [26]. On the contrary, $\dot{Q}_r$ remains almost constant ≈ 4 mW during the ramp. This would explain the coil heating observed in Fig. 7(h), in contrast with the case analysed in 3.1, when at the same temperature and ramp rate, but with applied currents well below the critical current of the coil, the temperature of the coil remained constant.

As expected, at 30 K the heating of the coil is more important than at 60 K. This is caused by several factors. In one hand, at 30 K the applied currents are much higher than at 60 K (with similar coil voltages). On the other hand, upon decreasing the temperature, the heat capacity decreases and the absolute thermal resistance increases, as it will be further analysed in the next section. Nevertheless, it must be remarked that resistive coil voltages above 250 μV and high applied currents were held for several seconds without triggering a quench.

Critical currents of superconductors are usually defined using the 1 μV/cm criterion. However, due to the uneven magnetic field distribution inside the coil, it should be preferable to use more restrictive criteria to define I_c [30,31], otherwise some regions may be well below their local I_c while others can withstand high voltages, which can cause local hot spots and, eventually, produce irreversible damage to the coil.

Fig. 9 compares the coil critical current values obtained experimentally using the 0.1 μV/cm criterion and the $I_c(T)$ values estimated with the modified load-line method explained in Section 3.2. It is worth noting the good correspondence between experimental and estimated values, with almost identical temperature dependence but with experimental values about 10% lower than numerical estimations. Some of the assumptions considered in the model could explain the observed differences: *i*) The current was assumed uniformly distributed in the winding, but in reality the differences of $I_c/w(z)$ would produce a redistribution of the current across the tape's width, which would then affect the magnetic field distribution in the winding [31]. *ii*) The $I_c(B,\theta)/w$ dependence was assumed to be independent of w. *iii*) In the numerical calculation, the lift factors, $I_c(T,B,\theta)/I_c(77\text{ K,self-field})$, have been obtained from experimental results measured in a different short sample [32]. That tape corresponds to the same type (SCS4050-AP) and was produced in the same reactor (M4), as the conductor used in this work. Nevertheless, several groups have reported differences among

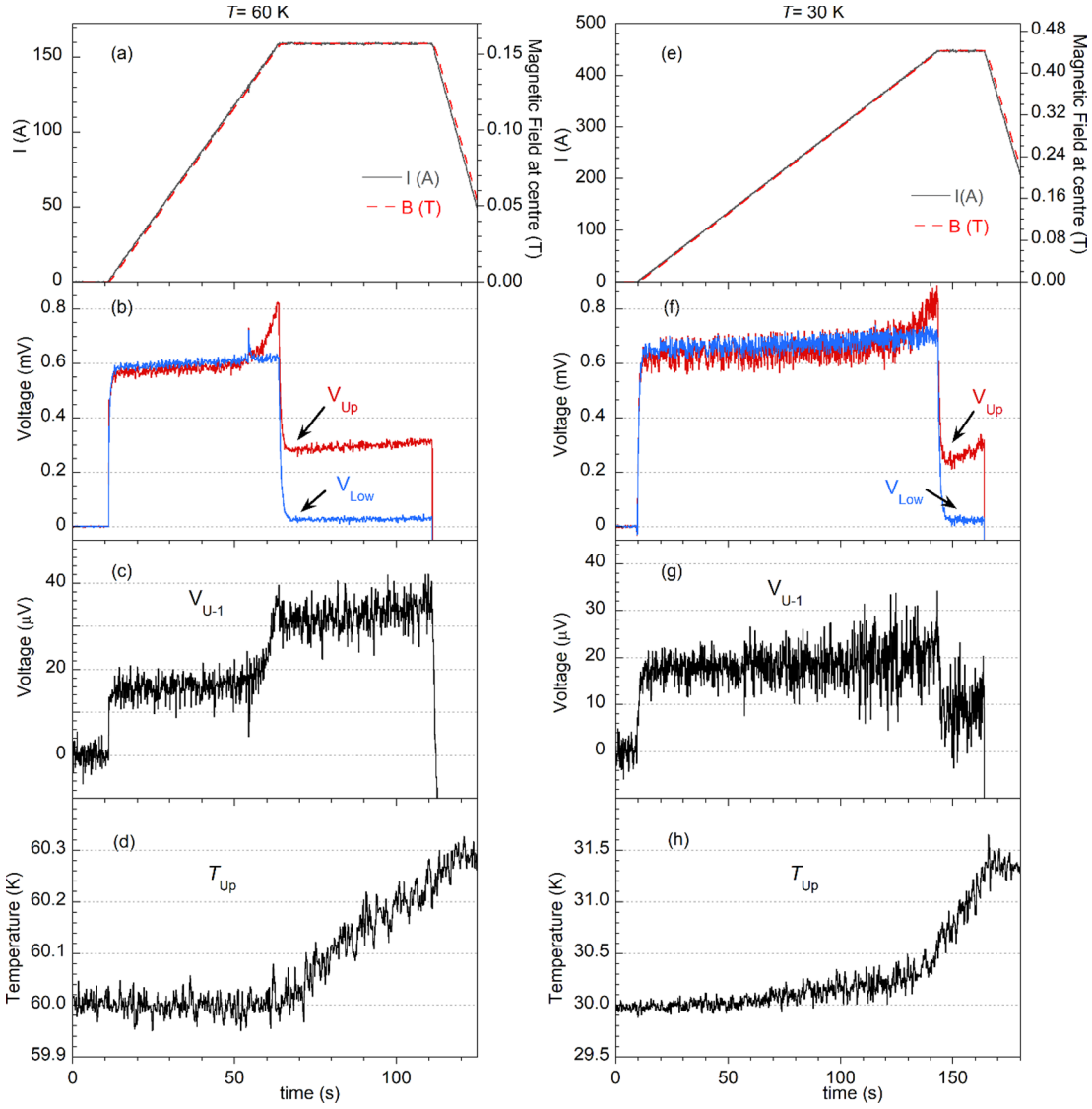

Fig. 7. Applied current, $I(t)$, magnetic field at the coil centre, $B_{centre}(t)$; voltages measured in both pancake coils ($V_{Up}(t)$ and $V_{Low}(t)$) and in the innermost turn of the upper pancake coil ($V_{U\text{-}1}$); and temperature T_{Up}, measured by the thermocouple TC-up (placed in the upper coil). Figs. (a)–(d) correspond to measurements at T = 60 K and current ramp rate of 3 A/s up to 159 A; (e)–(h) at T = 30 K and current ramp rate of 3.3 A/s up to 447 A.

identical nominal commercial tapes [34–36], which could be attributed to pinning centre density variations [36]. Therefore, the used $I_c(B,\theta)/w$ dependence can only be considered as typical but not universal.

3.4. Effect of thermal cycling and thermal properties

2G-HTS coils may suffer certain degradation of their superconducting properties if delamination of the tapes during thermal cycling occurs [37]. To analyse this effect, the coil voltage during current ramping above I_c was measured after subjecting the coil to a number of thermal cycles (N_{cycles}) between 300 K and cryogenic temperatures.

Fig. 10 shows the upper coil voltage $V_{Up}(t)$ at 60 K for identical linear current ramps up to 159 A at 3 A/s, after 3, 4 and 5 thermal cycles. The resistive voltage at 159 A increased from 280 μV to 390 μV from the third to the forth cycle, which in principle may indicate certain deterioration of the coil. Nevertheless, when heating up the system after this measurement, it was observed that the epoxy that joined the coil to the copper support plate was partially separated from the copper plate. Therefore, the coil and copper plate were reglued. When the system was subsequently cooled (N_{cycles} = 5), the measured resistive voltage V_{Up} decreased down to about 210 μV at the same conditions (see Fig. 10). Therefore, this indicates that the differences in the measured resistive voltage upon thermal cycling were not due to the coil degradation but to the inadequate epoxy adhesion to copper.

To analyse the properties of the thermal contact between the different parts of the DP coil, a constant power $\dot{Q}_{heater}$ = 0.1 W was applied to the heater glued to the uppermost surface of the coil (see in Fig. 1(b)). As seen in Fig. 11, this produces an increase of the temperatures in the upper, $T_{Up}(t)$, and lower, $T_{Low}(t)$, pancake coils. The temperature in the copper support was maintained constant by a temperature controller (see 2.2), so that all the system eventually reaches a steady state.

Thus, the absolute thermal resistance between the lower coil and the copper plate can be estimated as $R_{th(Low\text{-}Cu)} = \Delta T_{Low\text{-}Cu}/\dot{Q}_{heater}$, with $\Delta T_{Low\text{-}Cu} = T_{Low} - T_{Cu}$ at the steady state. Similarly, the absolute thermal resistance between the upper and lower coils $R_{th(Up\text{-}Low)} = \Delta T_{Up\text{-}Low}/\dot{Q}_{heater}$ with $\Delta T_{Up\text{-}Low} = T_{Up} - T_{Low}$. The obtained values $R_{th(Low\text{-}Cu)}$ = 7.6 K/W and $R_{th(Up\text{-}Low)}$ = 4.3 K/W at 60 K; increase to 12.6 and 5.9 K/W, respectively, at 30 K.

The corresponding thermal contact conductance values of the joint between the lower coil and the copper plate, h_j can be estimated using Eq. (1). In this case $\dot{Q} = \dot{Q}_{heater}$ = 0.1 W, $\Delta T = \Delta T_{Low\text{-}Cu}$ and A_c =

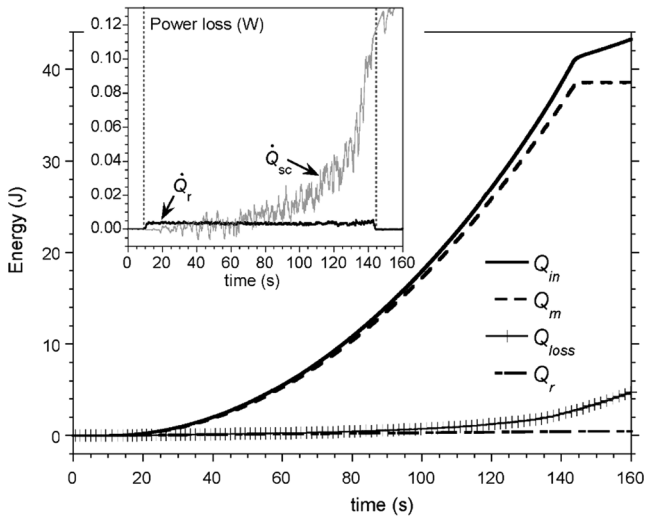

Fig. 8. Total energy supplied to the coil, $Q_{in}(t)$, energy loss, $Q_{loss}(t)$, magnetic energy stored in the coil, $Q_m(t)$, and energy dissipated by the currents flowing in the radial direction, $Q_r(t)$, calculated from experiments at 30 K, current ramp up to 447 A at 3.3 A/s. The inset shows the power loss contributions $\dot{Q}_r$ and $\dot{Q}_{sc}$ for the same experiment. The vertical dotted lines in the inset marks the beginning and the end of the current ramp.

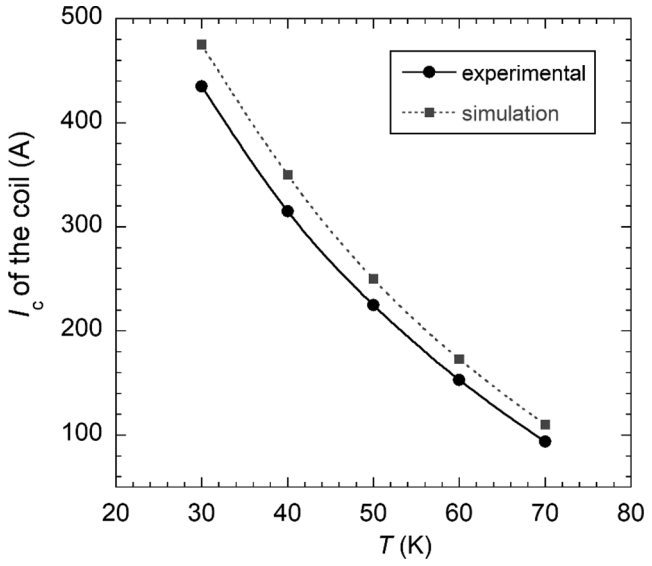

Fig. 9. Critical current of the DP coil obtained experimentally (using a 0.1 μV/cm criterion) compared with the estimated values using the modified load-line method explained in 3.2.

$\pi(D_{out}^2 - D_{in}^2)/4 = 11.3$ cm^2, and thus, we obtain values of $h_j = 116.3$ and 70.2 W m^{-2} K^{-1} at 60 K and 30 K, respectively. There are many factors that influence h_j, such as copper surface preparation, thickness and type of epoxy, area of the joint, etc. [38]. Nevertheless, considering the value of $h_j = 500$ W m^{-2} K^{-1} at 10 K reported for Cu/epoxy/Cu joints by other authors [38,39] (for $A_c = 1$ cm^2, epoxy SC5 and epoxy thickness of 80 μm), and the values obtained here for the electrically insulated thermal joints at the current lead heat sinks in Section 2.3, there is considerable scope for enhancing this thermal joint.

4. Conclusions

The thermal stability, thermal cycling and electromagnetic behaviour of a non-insulated (NI) conduction-cooled double pancake (DP) 2G-HTS coil have been studied between 5 K and 77 K, focusing on the analysis above 30 K. The DP coil was operated at high currents, both above and below the coil critical current, and in high vacuum conditions. The coil was epoxy impregnated after winding and subsequently glued with an epoxy resin to a copper support plate, which was anchored the second stage of a cryocooler.

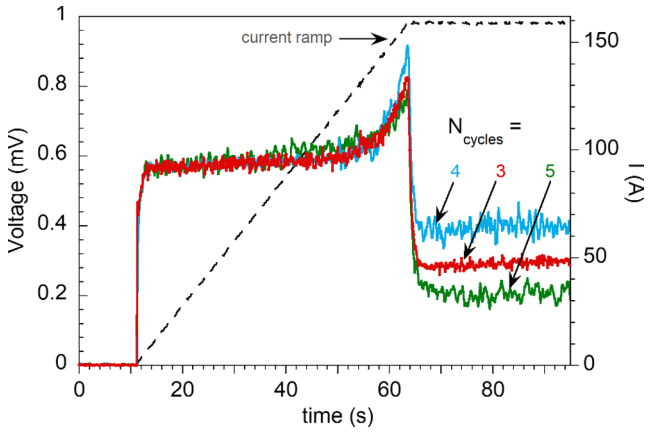

Fig. 10. $V_{Up}(t)$ measured at 60 K for three different thermal cycles, $N_{cycles} = 3$, 4 and 5 when ramping the current from 0 up to 159 A at 3 A/s and then kept constant. Note that measurement shown in Fig. 7(b) corresponds to $N_{cycles} = 3$.

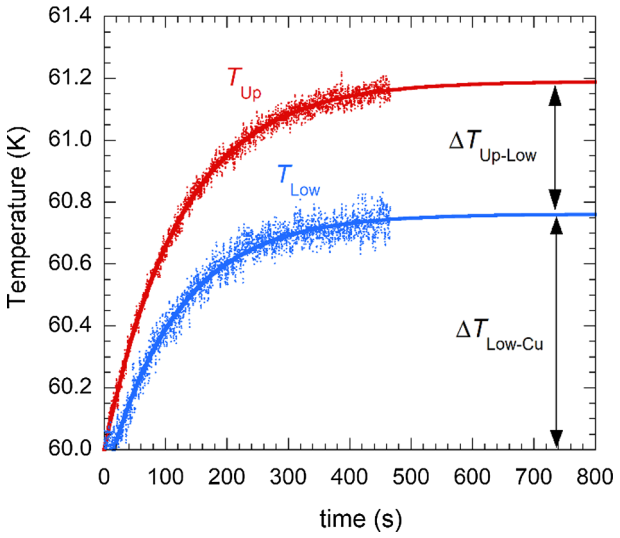

Fig. 11. Evolution of temperatures $T_{Up}(t)$ and $T_{Low}(t)$ when applying constant heating power $\dot{Q}_{heater} = 0.1$ W to the uppermost surface of the coil, and with the copper plate maintained at 60 K. Points correspond to experimental values and the continuous lines to exponential fits that give $\Delta T_{Low\text{-}Cu} = 0.76$ K and $\Delta T_{Up\text{-}Low} = 0.43$ K at the steady state.

The thermal stability of the whole cryogenic system was analysed, with especial attention to the behaviour of current leads, which were designed with two intermediate heat sinks. The electrically insulated thermal joints of the heat sinks, which have high thermal contact conductance ($h_j \approx 1800$ and 850 W m^{-2} K^{-1} at ≈ 80 K and ≈ 35 K, respectively) provides the necessary thermal stability to the system.

Charging and discharging tests of the coil have been performed and analysed using a simple equivalent circuit to estimate the contributions of turn-to-turn and magnetization losses during the ramp, for different ramp rates, obtaining good correspondence with the observed coil heating. The derived turn-to-turn contact resistance $R_t \approx 110$ μΩ cm^2 at 77 K and about half at 5 K, are of the order but in the upper bound of results reported by other groups in similar non-insulated 2G-HTS coils without epoxy resin impregnation.

A good correspondence between the experimental coil critical

currents and the estimated values, using a modified load-line method to account for the tape anisotropy, were found between 30 K and 70 K with almost identical temperature dependence, but experimental values ≈10% lower.

At 30 K, with applied overcurrents (currents above I_c) of 447 A that gave coil resistive voltages above 250 μV, it was possible to hold the system for several seconds without triggering a quench. Moreover, the coil was subjected to several thermal cycles from 300 K to the cryogenic operating temperatures without observing degradation of its superconducting properties, indicating the electro-thermal robustness of the NI manufacture.

Several experiments were performed to analyse the thermal contact between the different parts of the DP coil (i.e., copper support plate, and lower and upper coils). It was found that the joint between the coil and the support plate constitutes the weak-point of the coil system. This was due to an inadequate adhesion between copper and epoxy, and needs further work.

CRediT authorship contribution statement

A. Cubero: Investigation, Resources, Formal analysis, Writing - original draft. **A.B. Núñez-Chico:** Investigation, Formal analysis, Writing - review & editing. **R. Navarro:** Conceptualization, Methodology, Writing - review & editing. **L.A. Angurel:** Methodology, Resources, Writing - review & editing, Project administration. **E. Martínez:** Conceptualization, Formal analysis, Investigation, Resources, Writing - original draft, Project administration.

Declaration of Competing Interest

The authors declare that they have no known competing financial interests or personal relationships that could have appeared to influence the work reported in this paper.

Acknowledgements

This work was supported by projects ENE2017-83669-C4-1-R (MINECO/AEI/FEDER, EU) and ENE-2014-52105-R (MINECO/FEDER, EU) and by the Gobierno de Aragón “Construyendo Europa desde Aragón” (research group T54_17R). The authors acknowledge the use of Servicio General de Apoyo a la Investigación-SAI, University of Zaragoza.

References

[1] Barnes PN, Sumption MD, Rhoads GL. Review of high power density superconducting generators: Present state and prospects for incorporating YBCO windings. Cryogenics 2005;30:670.
[2] Abrahamsen AB, Mijatovic N, Seiler E, et al. Superconducting wind turbine generators. Supercond Sci Technol 2010;23(3):034019.
[3] Chen XY, Jin JX, Xin Y, Shu B, Tang CL, Zhu YP, Sun RM. Integrated SMES Technology for Modern Power System and Future Smart Grid. IEEE Trans Appl Supercond 2014;24(5):3801605.
[4] Haran KS, Kalsi S, Tabea Arndt T, et al. High power density superconducting rotating machines development status and technology roadmap. Supercond Sci Technol 2017;30:123002.
[5] Parizh M, Lvovsky Y, Sumption M. Conductors for commercial MRI magnets beyond NbTi: requirements and challenges. Supercond Sci Technol 2017;30:014007.
[6] Zhang K, Higley H, Liyang Y, et al. Tripled critical current in racetrack coils made of Bi-2212 Rutherford cables with overpressure processing and leakage control. Supercond Sci Technol 2018;31:105009.
[7] Rossi L, Badel A, Bajas H, et al. The EuCARD2 Future Magnets Program for Particle Accelerator High-Field Dipoles: Review of Results and Next Steps. IEEE Trans Appl Supercond 2018;28(3):8239658.
[8] Hahn S, Park DK, Bascuñán J, Iwasa Y. HTS Pancake Coils Without Turn-to-Turn Insulation. IEEE Trans Appl Supercond 2011;21(3):1592–5.
[9] Wang X, Hahn S, Kim Y, Bascuñán J, Voccio J, Lee H, Iwasa Y. Turn-to-turn contact characteristics for an equivalent circuit model of no-insulation ReBCO pancake coil. Supercond Sci Technol 2013;26:035012.
[10] Kim K, Jung S-J, Sung H-J, Kim G-H, Kim S, Lee S, et al. Operating characteristics of an insulationless HTS magnet under the conduction cooling condition. IEEE Trans Appl Supercond 2013;23(3):460150.
[11] Lee TS, Hwang YJ, Lee J, Lee WS, Kim J, Song SH, et al. The effects of co-wound Kapton, stainless steel and copper, in comparison with no insulation, on the time constant and stability of GdBCO pancake coils. Supercond Sci Technol 2014;27:065018.
[12] Wang Y, Song H, Xu D, Li ZY, Jin Z, Hong Z. An equivalent circuit grid model for no-insulation HTS pancake coils MgB_2 coil segment for MRI applications. Supercond Sci Technol 2015;28:045017.
[13] Jang JY, et al. Design, construction and 13 K conduction-cooled operation of a 3 T 100 mm stainless steel cladding all-REBCO magnet. Supercond Sci Technol 2017;30:105012.
[14] Yoon S, Cheon K, Lee H, Moon S-H, Kim S-Y, Kim Y, et al. The performance of the conduction cooled 2G HTS magnet wound without turn to turn insulation generating 4.1 T in 102 mm bore. Physica C 2013;494:242–5.
[15] Choi YH, Song JB, Yang DG, Kim YG, Hahn S, Lee HG. A novel no-insulation winding technique for high temperature superconducting racetrack coil for rotating applications: a progress report in Korea university. Rev Sci Instrum 2016;87:104704.
[16] Kim SB, Saitou A, Joo JH, Kadota T. The normal-zone propagation properties of the non-insulated HTS coil in cryocooled operation. Physica C 2011;471:1428–31.
[17] Zhang D, et al. Instrumentation, cooling and initial testing of a large, conduction-cooled, react-and-wind MgB2 coil segment for MRI applications. Supercond Sci Technol 2018;31:085013.
[18] Kim HS, Kovacs C, Rindfleisch M, Yue J, Doll D, Tomsic M, et al. Demonstration of a conduction cooled react and wind MgB_2 coil Segment for MRI. IEEE Trans Appl Supercond 2016;26(4):4400305.
[19] Ren L, Xu Y, Chen L, Wang Z, Qi D, Wang Z, et al. Study on the thermal characteristic of a 150 kJ/100 kW conduction-cooled HTS magnet. IEEE Trans Appl Supercond 2018;28(6):5701408.
[20] Song X, Mijatovic N, Kellers J, Bührer C, Rebsdorf AV, Hansen J, et al. A full-size high-temperature superconducting coil employed in a wind turbine generator setup. IEEE Trans Appl Supercond 2017;27(4):5201105.
[21] Dai Y, Yan L, Zhao B, Song S, Lei Y, Wang Q. Tests on a 6 T Conduction-Cooled Superconducting Magnet. IEEE Trans Appl Supercond 2006;16(2):961.
[22] Laskaris ET, Ackermann R, Doni B, Gross D, Herd K, Minas C. A Cryogen-Free Open Superconducting Magnet For Interventional MRI Applications. IEEE Trans Appl Supercond 1995;5(2):163.
[23] Watanabe K, Nishijima G, Awaji S, Takahashi K, Koyama K, Kobayashi N, et al. Performance of a Cryogen-Free 30 T-Class Hybrid Magnet. IEEE Trans Appl Supercond 2006;16(2):934.
[24] Awaji S, Watanabe K, Oguro H, Miyazaki H, Hanai S, Tosaka T, et al. First performance test of a 25 T cryogen-free superconducting magnet. Supercond Sci. Technol. 2017;30:065001.
[25] Ekin J. Experimental techniques for low-temperature measurements. Oxford, U.K: Oxford Univ. Press; 2006.
[26] Wang Y, Song H, Yuan W, Jin Z, Hong Z. Ramping turn-to-turn loss and magnetization loss of no-insulation $(RE)Ba_2Cu_3O_x$ high temperature superconductor pancake coil. J Appl Phys 2017;121:113903.
[27] Lu J, Goddard R. Han K and Hahn S Contact resistance between two REBCO tapes under load and load cycles. Supercond Sci Technol 2017;30:045005.
[28] Wilson MN. Superconducting Magnets, Oxford, U.K.: Oxford Univ. Press; 1987.
[29] Wimbush SC, Strickland NM. The Magnetic-Field Dependence of Critical Current: What We Really Need to Know. IEEE Trans Appl Supercond 2017; 27(4): 8000505.
[30] Zhang M, Kim J-H, Pamidi S, Chudy M, Yuan W, Coombs TA. Study of second generation, high-temperature superconducting coils: Determination of critical current. J Appl Phys 2012;111:083902.
[31] Liu ZY, Ou J, Grilli F, Schreiner F, Zermeño VMR, Min Zhang M, et al. Comparison of 2D simulation models to estimate the critical current of a coated superconducting coil. Supercond Sci Technol 2019;32:014001.
[32] Wimbush SC, Strickland NM. Critical current characterisation of SuperPower M4 Advanced Pinning 2G HTS superconducting wire; 2017. https://doi.org/10.6084/m9.figshare.3759318.v2.
[33] Núñez-Chico AB, Martínez E, Angurel LA, Navarro R. Enhanced quench propagation in 2G-HTS coils co-wound with stainless steel or anodised aluminium tapes. Supercond Sci Technol 2016;29:085012.
[34] Jirsa M, Rameš M, Ďuran I, Melíšek T, Kováč P, Viererbl L. Electric currents in REBaCuO superconducting tapes. Supercond Sci Technol 2017;30:045010.
[35] Tsuchiya K, Kikuchi A, Terashima A, Norimoto K, Uchida M, Tawada M, et al. Critical current measurement of commercial REBCO conductors at 4.2 K. Cryogenics 2017;85:1–7.
[36] Rossi L, Hu X, Kametani F, Abraimov D, Polyanskii A, Jaroszynkski J, et al. Electric currents in REBaCuO superconducting tapes. Supercond Sci Technol 2016;29:054006.
[37] Takematsu T, Hu R, Takao T, Yanagisawa Y, Nakagome H, Uglietti D, et al. Degradation of the performance of a YBCO-coated conductor double pancake coil due to epoxy impregnation. Physica C 2010;470:674–7.
[38] Gmelin E, Asen-Palmer M, Reuther M, Villar R. Thermal boundary resistance of mechanical contacts between solids at sub-ambient temperatures. J Phys D Appl Phys 1999;32:R19–43.
[39] Matsumoto DS, Reynolds Jr CL, Anderson AC. Thermal boundary resistance at metal–epoxy interfaces. Phys Rev. B 1977;16:3303–7.